Quark–gluon plasma phenomenology from anisotropic lattice QCD

Jon-Ivar Skullerud[*], Gert Aarts[†], Chris Allton[†], Alessandro Amato[†], Yannis Burnier[**], P. Wynne M. Evans[†], Pietro Giudice[‡], Simon Hands[†], Tim Harris[§], Aoife Kelly[*], Seyong Kim[¶], Maria Paola Lombardo[‖], Mehmet B. Oktay[††], Alexander Rothkopf[‡‡] and Sinéad M. Ryan[§]

[*]*Department of Mathematical Physics, Maynooth University, Maynooth, Co Kildare, Ireland*
[†]*Department of Physics, Swansea University, Swansea SA2 8PP, Wales*
[**]*Institut de Théorie des Phénomènes Physiques, Ecole Polytechnique Fédérale de Lausanne, CH–1015 Lausanne, Switzerland*
[‡]*Institut für Theoretische Physik, Universität Münster, D–48149 Münster, Germany*
[§]*School of Mathematics, Trinity College, Dublin 2, Ireland*
[¶]*Department of Physics, Sejong University, Seoul 143-747, Korea*
[‖]*INFN–Laboratori Nazionali di Frascati, I–00044 Frascati (RM), Italy*
[††]*Department of Physics and Astronomy, University of Iowa, Iowa City, Iowa 52242, USA*
[‡‡]*Institut für Theoretische Physik, Universität Heidelberg, Philosophenweg 16, D–69120 Heidelberg, Germany*

Abstract. The FASTSUM collaboration has been carrying out simulations of $N_f = 2+1$ QCD at nonzero temperature in the fixed-scale approach using anisotropic lattices. Here we present the status of these studies, including recent results for electrical conductivity and charge diffusion, and heavy quarkonium (charm and beauty) physics.

Keywords: Quark-gluon plasma, lattice QCD, conductivity, heavy quarkonium
PACS: 12.38Mh,12.38Gc,25.75.-q

INTRODUCTION

The heavy-ion collision experiments at RHIC and LHC have given a wealth of information about QCD matter at high temperatures, and have provided strong evidence for the existence of a deconfined state of matter, the quark–gluon plasma (QGP). Furthermore, it has been shown that at the energy densities reached in these experiments, this state of matter can be described well by nearly ideal hydrodynamics, and must hence be strongly coupled. A large amount of information has also been obtained about various probes of the QGP, including electromagnetic probes, high-energy jets and heavy quarks.

One of the outstanding challenges is to obtain a clear theoretical understanding of all the phenomena observed in the heavy-ion collisions. In particular, first-principles calculations of transport coefficients such as viscosity and conductivity would place the hydrodynamical description on a solid footing. Heavy quarkonia have been proposed as "thermometers" of the QGP, but this requires a precise knowledge of their dissociation rates as a function of temperature.

Lattice QCD is the method of choice for obtaining quantitative theoretical predictions for QCD matter at high temperature and zero or small net baryon density. However, to obtain information about real-time quantities such as transport coefficients and dissociation rates, analytical continuation of the imaginary-time information obtained from lattice simulation is necessary. This is in principle an ill-posed problem, but it can be addressed using Bayesian methods such as the maximum entropy method (MEM) [1] and the new bayesian reconstruction method of [2], or with alternative, model independent methods [3, 4].

All these methods require a fine resolution in the temporal direction to obtain reliable results. This may be done by using anisotropic lattices with a smaller spacing in time than in space. The FASTSUM collaboration has for a number of years been carrying out simulations on anisotropic lattices with dynamical fermions with this in mind. Here we present some of the most recent results from these simulations.

TABLE 1. Parameters for the 1st and 2nd generation ensembles. $\xi = a_s/a_\tau$ is the anisotropy; N_s is the number of spatial sites and L_s is the extent of the lattice in the spatial directions.

Gen	N_f	ξ	a_s (fm)	a_τ^{-1} (GeV)	m_π/m_ρ	N_s	L_s (fm)
1	2	6.0	0.162	7.35	0.54	12	1.94
2	2+1	3.5	0.123	5.63	0.45	24	2.94
						32	3.94

TABLE 2. Temporal lattice extents N_τ and temperatures T used in our simulations.

Gen 1			Gen 2		
N_τ	T (MeV)	T/T_c	N_τ	T (MeV)	T/T_c
80	92	0.42	128	44	0.24
32	230	1.05	48	117	0.63
28	263	1.20	40	141	0.76
24	306	1.40	36	156	0.84
20	368	1.68	32	176	0.95
18	408	1.86	28	201	1.09
16	459	2.09	24	235	1.27
			20	281	1.52
			16	352	1.90

SIMULATION AND ANALYSIS DETAILS

We have generated two sets of anisotropic lattice ensembles using improved Wilson-type fermions, see Table 1 for details. The 1st generation ensemble [5, 6] had $N_f = 2$ active flavours with $m_\pi \approx 500$MeV, while the 2nd generation ensemble has $N_f = 2+1$ active flavours with a physical strange quark and $m_\pi \approx 400$MeV. The 2nd generation parameters are the same as those used by the Hadron Spectrum Collaboration [7, 8], who have kindly allowed us to use their zero-temperature configurations for the purpose of these studies. The 2nd generation configurations as well as light and charm quark correlators were produced using the Chroma software system [9] with BAGEL optimisation [10].

For each parameter set we have generated gauge configurations at a range of temperatures, see table 2 for details. Note that the second generation includes temperatures both below and above the deconfinement transition. The pseudocritical temperature T_c was determined from the inflection point of the renormalised Polyakov loop, see [11, 12] for details.

Transport properties and spectral information are encoded in spectral functions $\rho(\omega,\vec{p})$, which are related to the euclidean correlators $G_E(\tau,\vec{p})$ that can be computed on the lattice through the integral relation

$$G_E(\tau,\vec{p}) = \int_0^\infty \rho(\omega,\vec{p}) K(\tau,\omega;T) \frac{d\omega}{2\pi}, \quad K(\tau,\omega;T) = \frac{\cosh[\omega(\tau-\frac{1}{2T})]}{\sinh\frac{\omega}{2T}} \tag{1}$$

for a system in thermal equilibrium. We have used the maximum entropy method with Bryan's algorithm and the modified kernel proposed in [13] to determine the most likely spectral function given our correlators. We have also employed the novel Bayesian method developed in [2], and will present results using this method in the beauty sector.

CONDUCTIVITY, CHARGE SUSCEPTIBILITY AND CHARGE DIFFUSION

The electrical conductivity is related to the low-frequency limit of the current–current spectral function,

$$\sigma = \frac{1}{6} \lim_{\omega\to 0} \frac{\rho_{em}(\omega)}{\omega}, \tag{2}$$

with

$$G_{ii}^{em}(\tau) = \int d^3x \langle j_i^{em}(\tau,\vec{x}) j_i^{em}(0,\vec{0})^\dagger \rangle = \int_0^\infty \rho_{em}(\omega) K(\tau,\omega) \frac{d\omega}{2\pi}, \tag{3}$$

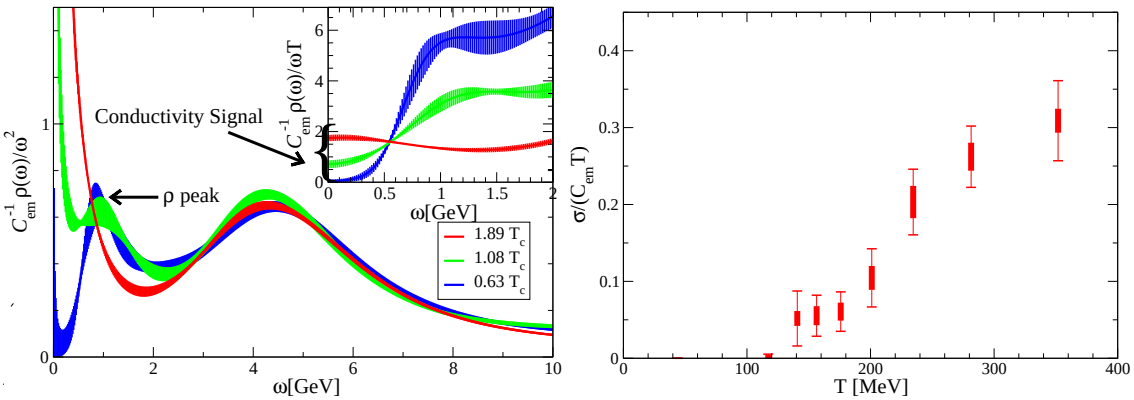

FIGURE 1. Left: light quark vector current spectral functions for three different temperatures below, near and above the pseudocritical temperature. The bands represent the statistical uncertainty. Right: the electrical conductivity (including contributions from u, d and s quarks) as a function of temperature. The boxes represent the uncertainties due to variations in the default model, while the error bars represent the total (systematic and statistical) uncertainty.

where $j_\mu^{em} = \sum_f (eq_f) j_\mu^f$ is the electromagnetic current operator and q_f are the quark charges in units of the elementary charge e. We have used the exactly conserved vector current on the lattice to compute $G_{ii}^{em}(\tau)$, see [14, 12] for details. In order to compare results obtained from simulations with different flavour content, in particular results from 2 (u, d) and 3 (u, d, s) flavours, the spectral functions and conductivity have been divided by the factor $C_{em} = \sum_f (eq_f)^2$, i.e. the sum of the squares of the quark charges.

We have also computed the susceptibilities of baryon number, isospin and electric charge as a function of temperature [15, 12]. These are of substantial phenomenological interest as they are related to the event-by-event fluctuations of these quantities in heavy-ion collisions, and may be used to locate the transition to the QGP and the critical endpoint in the temperature – chemical potential plane, if it exists.

Furthermore, the conductivity is directly related to the charge diffusion coefficient D_Q through the relation $D_Q = \sigma/\chi_Q$, where χ_Q is the electric charge susceptibility. While the analogous diffusion coefficient for heavy quarks has been widely studied, much less is known about diffusion of electric charge carried by light quarks. Here we present the first lattice calculation of this quantity. All the results in this section have been obtained with our 2nd generation ensemble.

In the left hand panel of figure 1 we show the light (u, d) quark contribution to $\rho_{em}(\omega)$ as a function of ω for three different temperatures: below, near and above the pseudocritical temperature T_c. Below T_c we can clearly identify the ρ meson peak in the spectral function, while this peak disappears at higher temperatures, in accordance with the ρ meson no longer being bound. Above T_c we find that $\rho(\omega)/\omega$ has a nonzero intercept with the $\omega = 0$ axis, signalling a nonzero value for the conductivity. The MEM analysis has been carried out using a default model $m(\omega) = m_0\omega(b+\omega)$, which allows for a finite, nonzero transport contribution while reproducing the continuum free spectral function at large ω.

The resulting values for the conductivity are shown in the right hand plot of figure 1. We have studied the stability of our results with respect to variations in the default model parameter b; the resulting systematic uncertainties are represented by the filled boxes in the figure, while the error bars represent the total (systematic and statistical) uncertainties. We have also investigated the stability of our results with respect to other systematics including the range and number of time slices included, and found that they are stable in all cases.

In the left panel of figure 2 we show our results for the isospin, electric charge and baryon susceptibilities as functions of temperature. They all show a similar behaviour, increasing rapidly near the crossover temperature T_c and approaching the value for a gas of free quarks and gluons at high temperature, as expected.

The right panel of figure 2 shows the charge diffusion coefficient D_Q as a function of temperature. Our results suggest that it has a minimum near T_c, with a value close to that predicted in AdS/CFT models, $D_Q = 1/(2\pi T)$.

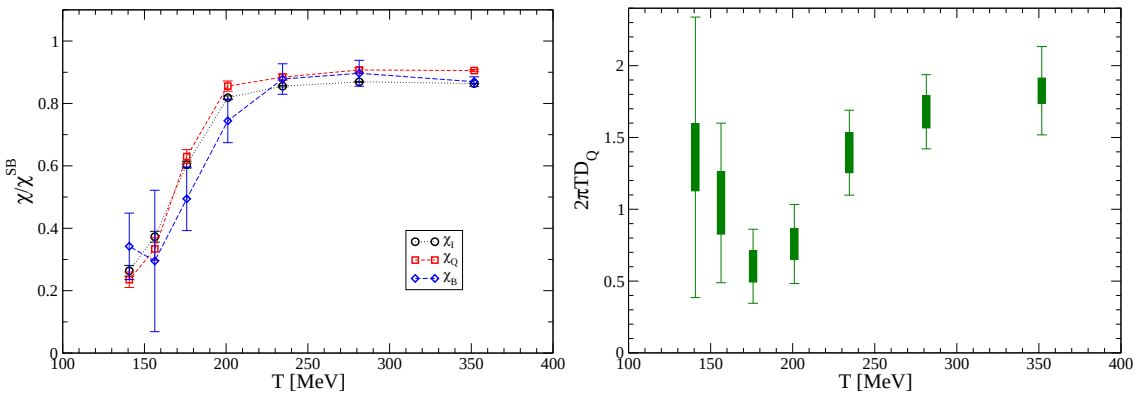

FIGURE 2. Isospin, electric charge and baryon susceptibility χ_I, χ_Q, χ_B, normalised by their values χ^{SB} in the noninteracting case (left) and charge diffusion coefficient D_Q (right) as function of temperature. These results include the contributions from u, d and s quarks. The meaning of the filled boxes and error bars are the same as in figure 1.

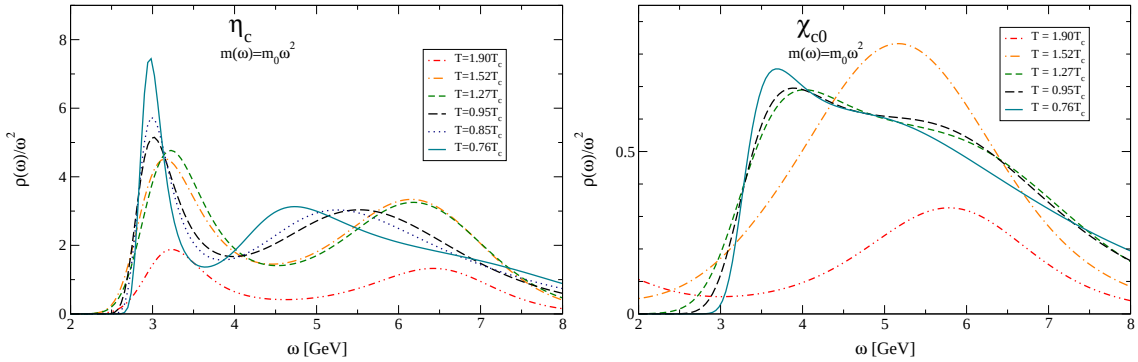

FIGURE 3. Charmonium spectral functions from the second generation ensemble. Pseudoscalar channel on the left, scalar channel on the right.

CHARM

Charmonium has been one of the most intensely studied probes in heavy-ion collisions since charmonium suppression was proposed as a signature of the QGP by Matsui and Satz [16]. There have been a number of lattice calculations of charmonium spectral functions, mostly in the quenched approximation [17, 18, 19, 20], but also recently using 2+1 light flavours [21]. We have previously studied charmonium on our 1st generation ($N_f = 2$) ensembles [22, 6]; here we will present results from our 2nd generation ensembles, as well as updated results for the momentum dependence of charmonium correlators from the 1st generation ensembles.

Charmonium at zero and nonzero momentum

Figure 3 shows charmonium spectral functions in the pseudoscalar (S-wave) and scalar (P-wave) channels from our second generation ensembles. Our results suggest that the S-wave ground state survives up to $T \approx 1.6T_c$, while the P-wave ground state melts close to T_c. This is consistent with our previous first generation results [22]. We have studied the dependence of these results on the default model used, and found that the results are stable for all but the highest temperature. We are in the process of analysing the data using the alternative Bayesian method of [2].

At nonzero momentum, the MEM reconstruction has much larger systematic uncertainties than at zero momentum [6, 23]. To circumvent this problem, we may instead compare the correlators at temperature T with the *reconstructed correlators* which result from integrating (1) using the kernel evaluated at T, but with a spectral function $\rho(\omega, \vec{p}; T_r)$ determined at a reference temperature T_r. The reference temperature is chosen to be relatively low so that the MEM

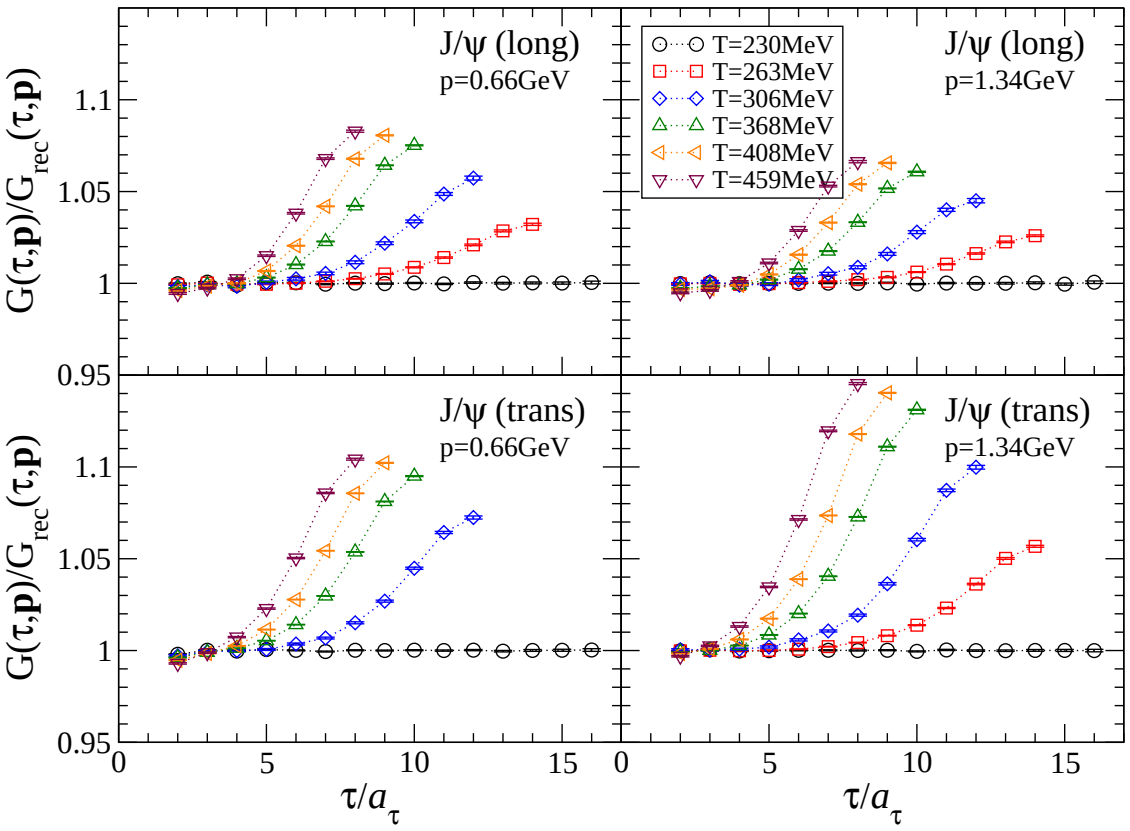

FIGURE 4. Reconstructed charmonium correlators in the longitudinal (top) and transverse (bottom) vector channel (1st generation), at two different momenta. The reference temperature is $T_r = 230$MeV ($N_\tau = 32$).

determination of $\rho(\omega, \vec{p}, T_r)$ is under control. Figure 4 shows this comparison for the vector channel at two different momenta with $T_r = 230$MeV. Note that the comparison is always made with the reconstructed spectral function for the same momentum. We see that the combined effect of the temperature and momentum is different in the longitudinal and transverse channel: while the thermal modifications in the longitudinal channel become smaller with increasing momentum, in the transverse channel they increase with the momentum, and are also larger in magnitude.

Charmonium potential

Nonrelativistic potential models have been widely used to study bound states of charm and beauty quarks both at zero and nonzero temperature. While it has long been known how their use can be given a firm foundation at zero temperature in effective field theory (pNRQCD), it is only recently that a similar understanding has begun to be developed in the high-temperature case [24, 25]. Most if not all high-temperature applications have so far been based on the potential between infinitely heavy (static) quarks, and it is not yet known how a finite quark mass will modify this.

We will take an alternative approach, assuming that the charmonium system can be described using a Schrödinger equation with a real potential, and determining the potential from the charmonium correlators that we compute on the lattice. Specifically, we compute point-split correlators with an operator $\Gamma = \{\gamma_\mu, \gamma_5\}$

$$C_\Gamma(\vec{r},\tau) = \sum_{\vec{x}} \langle \overline{\psi}(\vec{x},\tau) U(x, x+\vec{r}) \Gamma \psi(\vec{x}+\vec{r},\tau) \overline{\psi}(\vec{0},0) \Gamma^\dagger \psi(\vec{0},0) \rangle \,. \tag{4}$$

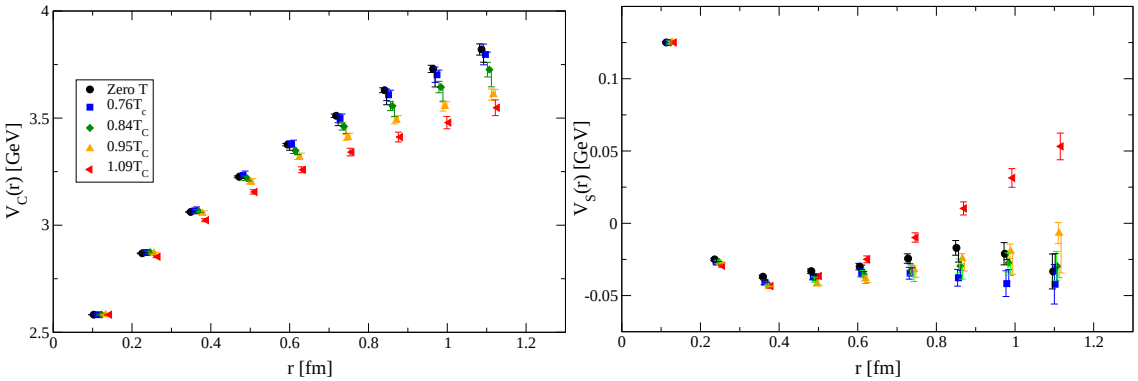

FIGURE 5. Charmonium potential. Left: central (spin-independent) potential; right: spin-dependent potential. The points are horizontally shifted for clarity. The two sets of error bars (to the left and right of the symbols) denote statistical and systematic (from variations in the time range used) uncertainties, respectively.

The potential $V_\Gamma(r)$ can then be determined using [26]

$$\frac{\partial C_\Gamma(r,\tau)}{\partial \tau} = \left(\frac{1}{m_c}\frac{\partial^2}{\partial r^2} - V_\Gamma(r)\right) C_\Gamma(r,\tau)\,, \tag{5}$$

which is valid for $\tau \ll 1/2T$. The vector and pseudoscalar potentials can be combined to produce the central (spin-independent) and spin-dependent potentials V_C and V_S,

$$V_C(r) = \frac{3}{4}V_{\gamma_\mu}(r) + \frac{1}{4}V_{\gamma_5}(5)\,, \quad V_S(r) = V_{\gamma_\mu}(r) - V_{\gamma_5}(r)\,. \tag{6}$$

The results are shown in figure 5. At low temperatures the central potential is well represented by the confining Cornell (linear + Coulomb) potential, while above T_c it becomes screened. The spin-dependent potential is attractive at intermediate distances with indications of a repulsive core. There appears to be a strong temperature dependence, also seen in our first generation results [27], which at present we have no clear understanding of.

BEAUTY

In recent years there has been an increased interest in b physics at high temperature and in heavy-ion collisions. In part this is because the energies reached at the LHC are such that $b\bar{b}$ pairs are created abundantly, whereas at RHIC and SPS they were relatively rare. Indeed, one of the early headline results from the heavy-ion collisions at CERN was the observation of sequential Υ suppression by the CMS collaboration [28].

Theoretically, the beauty system provides a cleaner probe of the QGP than the charm system, since effects such as regeneration and cold nuclear matter effects which may obscure the interpretation of the yields are much less significant. In addition, while the nonrelativistic approximation is marginal for charm quarks, it is clearly valid for bound states of beauty quarks. This allows us to use non-relativistic QCD (NRQCD), which is an effective theory obtained by integrating out the largest scale in the system, the heavy quark mass. In this case the kernel K in (1) simplifies to

$$K(\omega,\tau) = e^{-\omega\tau}\,. \tag{7}$$

Note that the heavy quark is explicitly not in thermal equilibrium here, and hence thermal (periodic) boundary conditions are not imposed. This has the additional advantage of doubling the number of independent points in the temporal direction.

We have previously applied the NRQCD formalism to our first generation ensembles in a series of papers [29, 30, 31, 32]. Here we will show results from our second generation ensembles [33]. The details of the simulation including the NRQCD action and the MEM reconstruction are presented in [33].

Our results [33] using the standard Bryan's implementation of MEM are shown in figure 6. We see that the S-wave (vector) ground state Υ survives up to the highest temperatures studied, while there is no evidence for any surviving P-

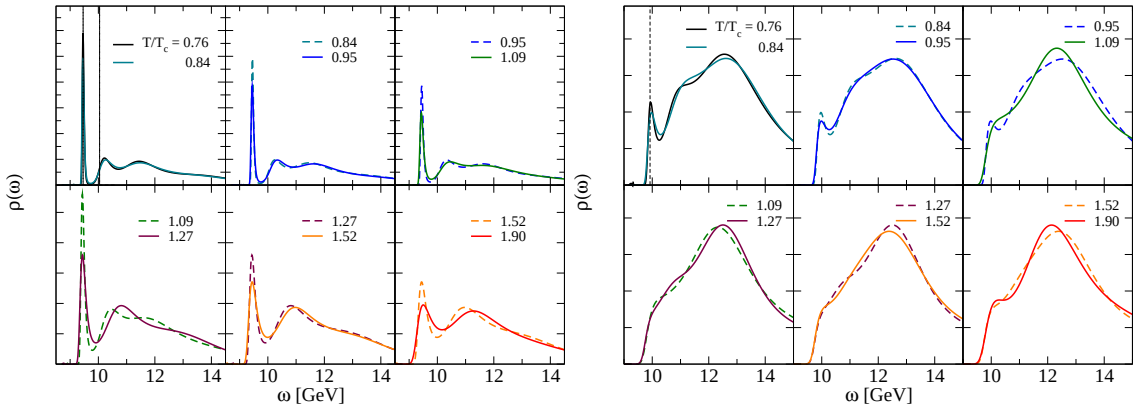

FIGURE 6. Beautonium spectral functions in the vector channel (left) and axial-vector channel (right), using the maximum entropy method [33].

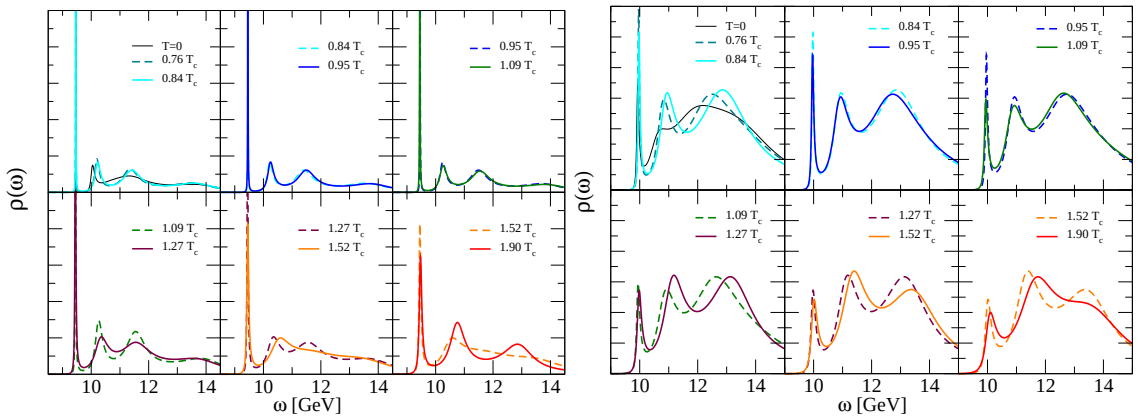

FIGURE 7. Beautonium spectral functions in the vector channel (left) and axial-vector channel (right), using the novel Bayesian method of [2].

wave (axial-vector) ground state for temperatures above T_c. This is consistent with our results from the first generation ensembles [30, 32].

Figure 7 shows our preliminary results using the novel Bayesian method of [2]. For the vector (S-wave) channel the results are in qualitative agreement with those from the maximum entropy method, although there are quantitative differences in the width of the ground state peak. For the axial-vector (P-wave) channel, on the other hand, the results in figure 7 suggest that the ground state survives until well into the QGP phase. This is in accordance with the results obtained in an analogous study using HotQCD ensembles [34]. We are currently investigating the source and significance of these differences, and this is discussed further in [35].

SUMMARY AND OUTLOOK

We have presented results from the FASTSUM collaboration's studies of high-temperature QCD using anisotropic lattices. Results have been obtained in the light quark, charm and beauty sectors, including the first results for the electrical conductivity and charge diffusion as a function of temperature below and above the phase transition, as well as charmonium and beautonium S and P wave states and the potential between charm quarks.

In the beauty sector, we are currently working on a detailed comparison of the two different Bayesian methods used in the spectral reconstructions in order to fully understand the differences between them. We are also looking at alternative methods which can complement this understanding. We hope that this will lead to quantitative results for the temperature-dependent mass shift and width of Υ states, which will assist in the interpretation of results from

heavy-ion collisions. In the charm sector, we have obtained preliminary results for D mesons at high temperature, and we are also planning to study charm diffusion using the same methods as for the conductivity and charge diffusion (see [23] for preliminary results). We are also investigating baryons at high temperature, as well as the real-time static quark potential using the methods of [2, 36].

Finally, we are in the process of generating new ensembles with the same quark masses and spatial lattice spacing, but with a smaller temporal lattice spacing. The finer temporal resolution will lead to a more reliable spectral reconstruction and bring some of the main systematic uncertainties associated with this under control. It will also allow us to reach higher temperatures, and will be the first step towards the aim of providing quantitative predictions for spectral and transport properties of the QGP, that is results in the continuum limit with physical or near-physical quark masses.

ACKNOWLEDGMENTS

This work is undertaken as part of the UKQCD collaboration and the STFC funded DiRAC Facility. We acknowledge the PRACE grants 2011040469 and Pra05_1129, European Union Grant Agreement number 238353 (ITN STRONGnet), the Irish Centre for High-End Computing, SFI grants 08-RFP-PHY1462 (JIS) and 11-RFP.1-PHY-3201 (TH and SMR), IRC (AK), Swansea University (AA), STFC, the Wolfson Foundation (GA), the Royal Society (GA), the Leverhulme Trust (GA and CA), SNF grant PZ00P2–142523 (YB) and the Research Foundation of Korea, grant No. 2010-002219 (SK) for support.

REFERENCES

1. M. Asakawa, T. Hatsuda, and Y. Nakahara, *Prog. Part. Nucl. Phys.* **46**, 459–508 (2001), hep-lat/0011040.
2. Y. Burnier, and A. Rothkopf, *Phys.Rev.Lett.* **111**, 182003 (2013), 1307.6106.
3. G. Cuniberti, E. De Micheli, and G. A. Viano, *Commun.Math.Phys.* **216**, 59–83 (2001), cond-mat/0109175.
4. Y. Burnier, and M. Laine, *Eur.Phys.J.* **C72**, 1902 (2012), 1201.1994.
5. R. Morrin, A. Ó Cais, M. Peardon, S. M. Ryan, and J.-I. Skullerud, *Phys. Rev.* **D74**, 014505 (2006), hep-lat/0604021.
6. M. B. Oktay, and J.-I. Skullerud (2010), 1005.1209.
7. R. G. Edwards, B. Joó, and H.-W. Lin, *Phys.Rev.* **D78**, 054501 (2008), 0803.3960.
8. H.-W. Lin, et al., *Phys.Rev.* **D79**, 034502 (2009), 0810.3588.
9. R. G. Edwards, and B. Joó, *Nucl.Phys.Proc.Suppl.* **140**, 832 (2005), hep-lat/0409003.
10. P. A. Boyle, *Comput.Phys.Commun.* **180**, 2739–2748 (2009).
11. C. Allton, G. Aarts, A. Amato, W. Evans, P. Giudice, et al., *PoS* **LATTICE2013**, 151 (2014), 1401.2116.
12. G. Aarts, C. Allton, A. Amato, P. Giudice, S. Hands, and J.-I. Skullerud (2014), 1412.6411.
13. G. Aarts, C. Allton, J. Foley, S. Hands, and S. Kim, *Phys.Rev.Lett.* **99**, 022002 (2007), hep-lat/0703008.
14. A. Amato, G. Aarts, C. Allton, P. Giudice, S. Hands, and J.-I. Skullerud, *Phys.Rev.Lett.* **111**, 172001 (2013), 1307.6763.
15. P. Giudice, G. Aarts, C. Allton, A. Amato, S. Hands, and J.-I. Skullerud, *PoS* **LATTICE2013**, 492 (2014), 1309.6253.
16. T. Matsui, and H. Satz, *Phys. Lett.* **B178**, 416 (1986).
17. M. Asakawa, and T. Hatsuda, *Phys. Rev. Lett.* **92**, 012001 (2004), hep-lat/0308034.
18. T. Umeda, K. Nomura, and H. Matsufuru, *Eur. Phys. J.* **C39S1**, 9–26 (2005), hep-lat/0211003.
19. S. Datta, F. Karsch, P. Petreczky, and I. Wetzorke, *Phys. Rev.* **D69**, 094507 (2004), hep-lat/0312037.
20. H. Ding, A. Francis, O. Kaczmarek, F. Karsch, H. Satz, et al., *Phys.Rev.* **D86**, 014509 (2012), 1204.4945.
21. S. Borsányi, S. Dürr, Z. Fodor, C. Hoelbling, S. D. Katz, et al., *JHEP* **1404**, 132 (2014), 1401.5940.
22. G. Aarts, C. Allton, M. B. Oktay, M. Peardon, and J.-I. Skullerud, *Phys. Rev.* **D76**, 094513 (2007), 0705.2198.
23. A. Kelly, J.-I. Skullerud, C. Allton, D. Mehta, and M. B. Oktay, *PoS* **LATTICE2013**, 170 (2014), 1312.0791.
24. Y. Burnier, M. Laine, and M. Vepsäläinen, *JHEP* **0801**, 043 (2008), 0711.1743.
25. N. Brambilla, J. Ghiglieri, A. Vairo, and P. Petreczky, *Phys.Rev.* **D78**, 014017 (2008), 0804.0993.
26. S. Aoki, et al., *PTEP* **2012**, 01A105 (2012), 1206.5088.
27. P. W. M. Evans, C. R. Allton, and J. I. Skullerud, *Phys.Rev.* **D89**, 071502 (2014), 1303.5331.
28. S. Chatrchyan, et al., *Phys.Rev.Lett.* **109**, 222301 (2012), 1208.2826.
29. G. Aarts, S. Kim, M. P. Lombardo, M. B. Oktay, S. M. Ryan, et al., *Phys.Rev.Lett.* **106**, 061602 (2011), 1010.3725.
30. G. Aarts, C. Allton, S. Kim, M. P. Lombardo, M. B. Oktay, et al., *JHEP* **1111**, 103 (2011), 1109.4496.
31. G. Aarts, C. Allton, S. Kim, M. P. Lombardo, M. B. Oktay, et al., *JHEP* **1303**, 084 (2013), 1210.2903.
32. G. Aarts, C. Allton, S. Kim, M. P. Lombardo, S. M. Ryan, and J.-I. Skullerud, *JHEP* **1312**, 064 (2013), 1310.5467.
33. G. Aarts, C. Allton, T. Harris, S. Kim, M. P. Lombardo, et al., *JHEP* **1407**, 097 (2014), 1402.6210.
34. S. Kim, P. Petreczky, and A. Rothkopf (2014), 1409.3630.
35. T. Harris, et al., *PoS* **LATTICE2014** (2014).
36. Y. Burnier, O. Kaczmarek, and A. Rothkopf (2014), 1410.2546.